

## Surface heating in relation to air temperature, wind and turbulence in an urban street canyon

B. Offerle · I. Eliasson · C. S. B. Grimmond ·  
B. Holmer

Received: 24 October 2005/Accepted: 22 May 2006  
© Springer Science+Business Media B.V. 2006

**Abstract** Wind and temperature measurements from within and above a deep urban canyon (height/width = 2.1) were used to examine the thermal structure of air within the canyon, exchange of heat with the overlying atmosphere, and the possible impacts of surface heating on within-canyon air flow. Measurements were made over a range of seasons and primarily analysed for sunny days. This allowed the study of temperature differences between opposing canyon walls and between wall and air of more than 15°C in summer. The wall temperature patterns follow those of incoming solar radiation loading with a secondary daytime effect from the longwave exchange between the walls. In winter, the canyon walls receive little direct solar radiation, and temperature differences are largely due to anthropogenic heating of the building interiors. Cool air from aloft and heated air from canyon walls is shown to circulate within the canyon under cross-canyon flow. Roofs and some portions of walls heat up rapidly on clear days and have a large influence on heat fluxes and the temperature field. The magnitude and direction of the measured turbulent heat flux also depend strongly on the direction of flow relative to surface heating. However, these spatial differences are smoothed by the shear layer at the canyon top. Buoyancy effects from

---

B. Offerle (✉) · I. Eliasson · B. Holmer  
Urban Climate Group, Physical Geography, Earth Sciences Centre, PO Box 460  
SE-405 30 Göteborg, Sweden  
e-mail: bofferle@yahoo.com

C. S. B. Grimmond  
Department of Geography, Indiana University, Bloomington USA

C. S. B. Grimmond  
Environmental Monitoring and Modelling Group, Geography, King's College London, London,  
UK

the heated walls were not seen to have as large an impact on the measured flow field as has been shown in numerical experiments. At night canyon walls are shown to be the source of positive sensible heat fluxes. The measurements show that materials and their location, as well as geometry, play a role in regulating the heat exchange between the urban surface and atmosphere.

**Keywords** Buoyancy · Heat flux · Surface temperature · Urban canyon · Wind field

## 1 Introduction

The landscape of dense urban areas can be described by units of a street flanked by buildings to form a ‘canyon’ (Oke 1987). Although there may exist considerable variation in building geometry the street canyon has proved useful as a unit of analysis in urban climatology (Arnfield 2003). Earlier research on street canyons that focused on wind, radiation, and energy balance regimes (for example, Dabbert et al. 1973; Nunez and Oke 1977) demonstrated these to be strongly linked to geometry. This geometry is often described by a single parameter, the canyon aspect ratio ( $H/W$ ). For incoming solar radiation and the heating of canyon surfaces, the orientation of the canyon relative to the solar path is also critical in determining the timing and extent to which surfaces receive direct sunlight. These factors to a large extent control the thermal response of the canyon. For larger areas of a city the thermal response is a function of the aggregation of these urban canyon units or an ‘average’ canyon (e.g. Masson 2000).

For an east–west (E–W) oriented canyon, the differential heating of surfaces is largely a function of latitude and time of year. Nakamura and Oke (1988) observed maximum surface–air temperature differences from the canyon floor of around 12–14°C and between sunlit wall and air of around 8–9°C. For a north–south (N–S) oriented canyon, the canyon floor may receive little direct radiation if the canyon is deep, but large differences in temperature between opposing façades may be observed as part of the diurnal course. The sun first heats the west wall of the canyon and then after solar noon the east wall, with the largest diurnal differences occurring early or late in the day, up to 20°C for the upper portion of the walls for a street canyon in Nantes, France (Louka et al. 2002). This usage of ‘west’ and ‘east’ specifies the canyon as the reference, although in the literature sometimes the building is used as a reference, so the east-facing canyon wall is the west wall of the building (Voogt and Oke 1998).

Numerous studies have shown that the geometry of the urban canyons reduces the reflected radiant energy leaving the canyon due to the multiple reflections that occur (Aida 1982; Arnfield 1982; Kondo et al. 2001; Sailor and Fan 2001; Harman et al. 2004a). For example, Aida (1982) and Aida and Gotoh (1982) showed that the effective bulk albedo decreases with increasing aspect ratios at least up to  $H/W = 2$ . Within the canyon, the geometry can reduce the differences in longwave emission between the walls (Harman et al. 2004a).

Recent research has shown that while sensible heat fluxes from roofs dominate the surface atmosphere heat exchange in the daytime, stored heat released from the walls within urban canyons can maintain neutral to unstable conditions over dense urban areas at night (Christen and Vogt 2004; Grimmond et al. 2004; Salmond et al. 2005; Offerle et al. 2006). The representation of urban surface fluxes in numerical models is

a topic of much recent attention for improving numerical weather prediction and air pollution dispersion modelling (Masson 2000; Martilli et al. 2002; Best 2005). Often a multinode resistance model is used to determine heat fluxes from within the canyon to the surface layer (e.g. Masson 2000; Kusaka et al. 2001). This approach implies that heat fluxes in the surface layer, spatially averaged by the action of turbulence, are well represented by fluxes from different surfaces within street canyons, being first mixed in the canyon air, then blended with fluxes from roofs above the canopy layer. The good performance of such models for estimating local-scale fluxes demonstrates the accuracy of such an approach (Masson et al. 2002) and scale-model studies have been used to validate the method (Harman et al. 2004b).

In one of the few observational studies that has linked the temperature distribution in a street canyon to the flow regime, Nakamura and Oke (1988) showed the penetration of cooler air from aloft and the characteristics of the vortex circulation. However, this interpretation was inferred from a single within-canyon wind measurement.

As shown by numerical modelling and wind-tunnel studies, differential heating of the surfaces within a street canyon may influence the flow pattern, and may be particularly important for the dispersal of pollutants in urban canyons. Thermal impacts on the flow regime are expected to be greatest when wind speeds are weak, or buoyancy forces relatively more important than inertial forces (Kovar-Panskus et al. 2002). This is often examined in the context of a Froude number, which relates the relative strength of inertial to buoyancy forces (Sini et al. 1996; Kovar-Panskus et al. 2002).

Simulated small-scale flows within the urban canopy to examine the effects of the wall heat flux due to the solar heating of ground or building walls showed that an upward buoyancy flux due to a heated windward wall opposes the downward advection and divides the flow structure into two counter-rotating cells (Sini et al. 1996). If the leeward wall is heated the effect is the opposite with buoyancy forces enhancing the vortex circulation (Baik and Kim 1999). Qualitatively similar results to Sini et al. (1996) were presented by Kovar-Panskus et al. (2002) from a wind-tunnel study at Froude numbers an order of magnitude lower. Although the vortex centre was displaced upwind, they reported little influence of wall temperature on the air temperature distribution and only weak secondary flow close to the ground. Little evidence was found that buoyancy forces induce a widespread upward motion (Kovar-Panskus et al. 2002), which is in agreement with results from balloon observations ( $H/W = 1.4$ ) in Nantes, France (Vachon et al. 1999). The Nantes study showed that a thin thermal layer extended out 0.2 m from the walls, with maximum intensity 20 mm from the heated wall. Balloons released near ground level tended to remain close to the surface except when they came very near the heated wall, whereby they rose along the wall (Kovar-Panskus et al. 2002). However, counter-rotating cells were not observed. Numerical simulations with bottom heating show multiple vortex development for a range of canyon aspect ratios (Kim and Baik 2001).

The objectives of this paper are to investigate the observed thermal structure (air and surface temperatures) within an urban street canyon and to examine its linkages to seasonality, air flow and heat flux both within and above the canyon. Modelled heat fluxes from the different surfaces are used to examine how the different surfaces contribute to the observed fluxes. The wind field is analysed to determine whether any buoyancy effects are apparent in the mean flow.

## 2 Methods

### 2.1 Site and measurements

Observations were conducted in a street canyon ( $H/W = 15/7.1 = 2.1$ ) in central Gothenburg, Sweden ( $57^{\circ}42' \text{ N}$ ,  $11^{\circ}58' \text{ E}$ ). The street, which runs approximately N–S ( $340^{\circ}$ ), is paved with cobbles and flanked by approximately equal height buildings. All the measurements were taken at or near the midpoint of a 50-m long block made up of four buildings. Vehicular traffic is light and vehicle speeds are restricted. The block had a 15-m mast located at the N–S midpoint and a second 15-m mast on the roof of the north building of the west wall of the canyon; a schematic of the instrumentation set-up is shown in Fig. 1. Wind velocity ( $u, v, w$ ) and temperature ( $T_v$ , sonic virtual temperature) measurements were made by ultrasonic anemometers (RM Young 81000) at 11 locations within the canyon, three above the roof and one around roof level (C6) (Fig. 1). The digital sonic output (10 Hz mean from an internal 200 Hz signal) was recorded for later processing. Unshielded thermocouples (TC) (Omega, T-type, 0.127 mm), co-located with each sonic on its north side, were used for air temperature ( $T_a$ ) measurements made at 1 Hz. All other measurements are made at 0.2 Hz. Surface temperature measurements were made by thermocouples (0.25 mm) affixed to the surface with a thin layer of adhesive. On the brick wall surfaces, finely crushed brick was mixed in with the adhesive. The wall TCs were mounted in vertical profiles (within  $\pm 0.3 \text{ m}$ ) directly opposite one another on the north-west and south-east buildings. An additional TC was set at 8 m (duplicate height) on the north-east building, which had a rough plastered surface. Additional TCs were added in 2004 to provide denser vertical sampling, mainly on the west wall (Fig. 1). Radiation components were measured with four-component radiometers (Kipp & Zonen CNR1) at 10 m above the roof, near the canyon top and at the lowest measurement level in the canyon. Two additional radiometers were oriented normal to the walls on either side of the canyon. The site location, surroundings and wind field measurements and processing are more completely described in Eliasson et al. (2005).

Instruments were compared after the conclusion of measurements at an open site. Data were acquired in the same manner as during the field experiment and then fitted to an ensemble value using linear regression analysis. After correction to this value, root-mean-square errors (RMSE) were less than  $0.05^{\circ}\text{C}$  for air temperature, and less than  $5 \text{ W m}^{-2}$  for all radiation components. With the exception of two surface temperature sensors, RMSE were also less than  $0.05^{\circ}\text{C}$ . Horizontal wind speeds were in agreement with the manufacturer's stated accuracy ( $\pm 1\% \text{ RMS } \pm 0.05 \text{ m s}^{-1}$ ).

### 2.2 Data classification and analysis

To analyse the data with respect to periods when large temperature gradients could exist between surface and air, and between canyon walls, data were classified into predominately 'sunny' and 'non-sunny' days for the period July 2003–August 2004. The initial criterion for sunny days was a daily clearness index above 0.6 ( $k_T = \sum K \downarrow / \sum I_0$ , where  $K \downarrow$  is the measured global solar radiation and  $I_0$  is the exoatmospheric radiation on a horizontal surface). Data from these days were examined to ensure that  $K \downarrow$  showed little variation due to changes in cloudiness. Incoming longwave was also examined to ensure that nights were free of low clouds. Data were sorted into 3-month periods, with summer covering June–August (19 sunny days) and winter from

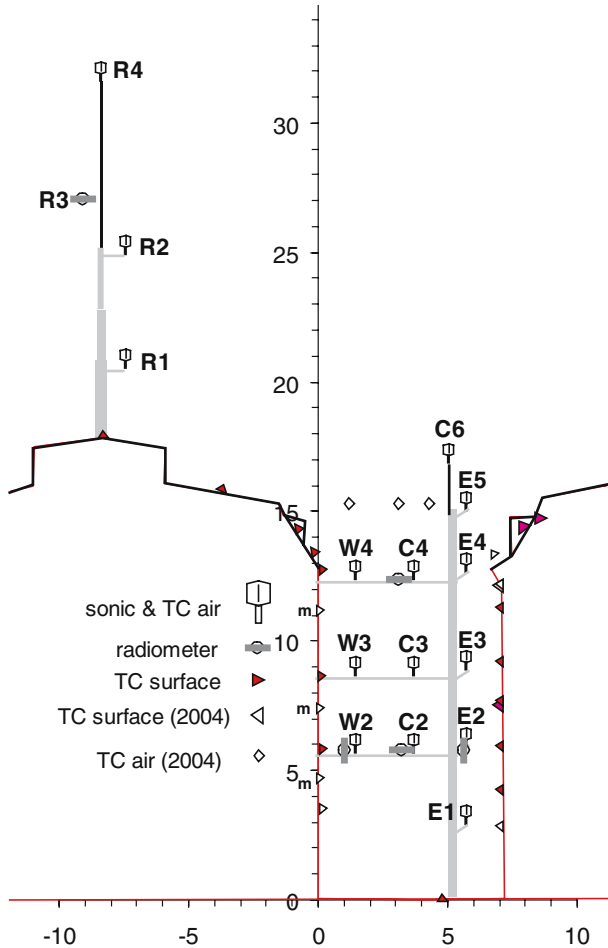


**Fig. 1** Schematic of canyon and instrumentation. The instrument positions are labelled ‘W’, ‘C’, ‘E’ or ‘R’ corresponding to west, centre, east and rooftop, respectively. All sonics have a co-located thermocouple (TC) for air temperature measurement. Year is given for instruments installed in 2004. Darker lines on the buildings indicate a metal roof surface. Wall TCs labelled with ‘m’ are also on metal surfaces

December–February (10 sunny days). The autumn and spring periods include 27 sunny days. Cross canyon flow was defined as within  $\pm 30^\circ$  of perpendicular to the canyon long axis with wind direction specified by the top level sonic (R4). All data presented are hourly averages.

To examine the relation between incoming solar radiation and canyon surface temperature, it was necessary to employ a model since the radiation components normal to the vertical surfaces were measured at only one height. Additionally, since the radiometers were located at a distance from the wall (1 m) they do not perfectly mimic the radiation balance at the walls’ surfaces. Global, direct and diffuse solar radiations are calculated using the Bird and Hulstrom (1981) model. Incident diffuse shortwave is weighted by the sky view factor ( $\psi_s$ ) at each point (Oke 1987) and access to direct

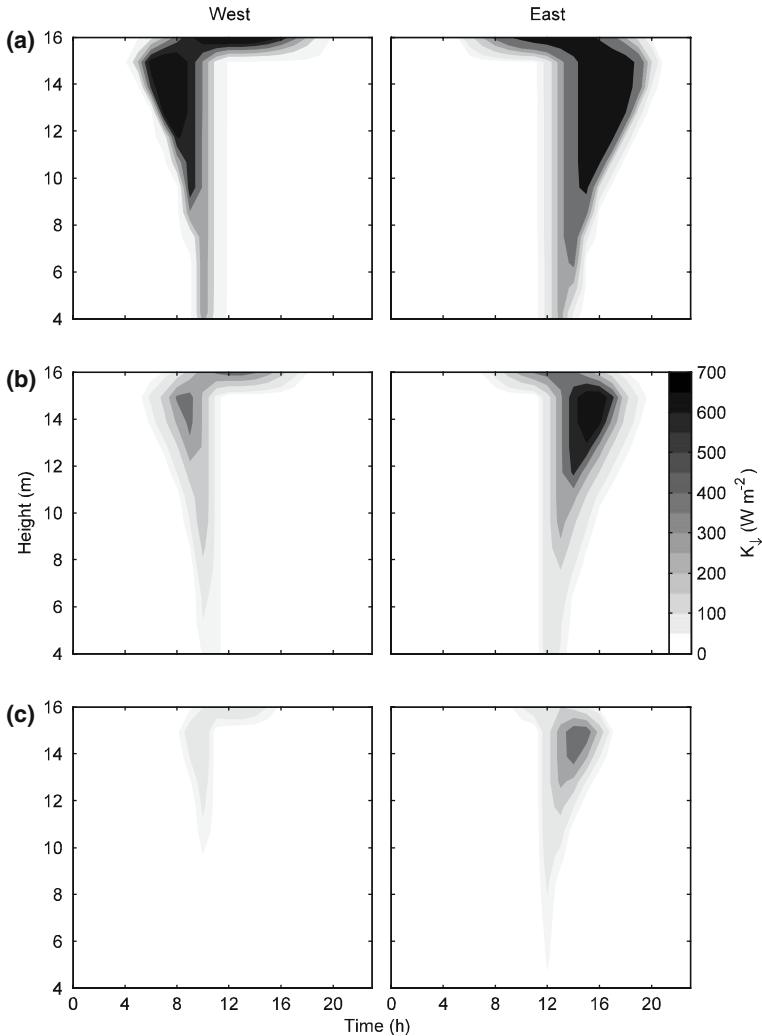


**Fig. 2** Simulated global solar radiation ( $K_{\downarrow}$ ) on canyon surfaces for the average of all sunny days in each subset: (a) summer, (b) spring and autumn, (c) winter

shortwave is determined by ray tracing at azimuth intervals of  $0.1^{\circ}$  for a symmetric infinite canyon of the same aspect ratio ( $H/W = 2.1$ ) as the study canyon. Global radiation was modelled at 1 m intervals on each wall (1–15 m), and at one point each for the roof (16 m) and street (0 m). All surfaces were treated as either horizontal (roof and street) or vertical (walls). Although the model does not consider reflections or three-dimensional effects, it provides the general spatial and temporal patterns for incoming solar radiation. Figure 2 shows modelled incident global solar radiation on canyon surfaces for the average of all sunny days in each subset. The highest shortwave loading occurs on the uppermost wall portion for much of the year. Due to the street orientation, the canyon walls receive substantially different incoming solar radiation during the diurnal cycle with the east wall receiving greater loading, more

notably in spring or autumn. Due to the low solar elevation at this latitude and the canyon depth, the street receives direct radiation for only a short time period during midday for much of the year. Between November 1 and March 1, the street and west wall receive little direct solar radiation.

### 2.3 Thermal structure

Information about the temperature distribution in the canyon is known from a large but limited number of temperature measurements within the canyon. The continuous measurements are made primarily within a single plane across the canyon (east–west and vertical). Therefore the data are analysed with respect to this  $x$  (west–east) – $z$  (vertical) plane. To better visualize the temperature structure in relation to the wind and turbulence fields, discussed in Sect. 3.3, some assumptions and interpolation were necessary. Air temperatures within the canyon were linearly interpolated to a regular grid within the boundary defined by the physical locations of the sensors (Fig. 1). Air temperature at R4 was assumed to be horizontally homogeneous at the sensor height and the lowest measured temperature (E1) was assigned across the canyon at that height. Wall surface temperatures were interpolated to a regular interval, again constrained by the physical locations of the sensors. Below 13 m height, only wall TCs on brick surfaces were included in the seasonal analysis to maintain consistency in materials. This excludes three TCs added in 2004 and marked in Fig. 1. Surface temperatures at the top part of the canyon (the sloped metal roof) were determined by the average of the sensors located on these portions of the roof. The lower boundary condition across the canyon (street) was fixed by the radiometric surface temperature measured at C2 ( $T_{\text{road}}$ ). The 50% field of view or source area for this measurement therefore includes the lowest 2 m of wall surface.

### 2.4 Turbulent heat flux

The turbulent transfer of heat within the canyon and from the canyon to the above atmosphere is critical for the temperature distribution in the canyon and the integrated response of the canyon unit. In Sects. 3.2. and 3.3 we will examine the relation between surface temperature, air temperature and turbulence within the canyon. Kinematic turbulent heat fluxes are computed as the covariance of wind vector with the sonic temperature (e.g. for vertical heat fluxes  $H = \overline{w'T'_v}$ , where the overbar denotes a time average), but is not corrected for density effects (e.g. Schotanus et al. 1983) so slightly overestimates the turbulent sensible heat flux. The information from these measurements is more valuable if the footprints for each sonic can be determined. For eddy covariance measurements within a homogeneous surface layer, the ‘footprint’ or source area for the measurement, i.e. what the instrument sees, can be readily computed (Schmid 2002). Within the canyon and near the canyon top, the flux footprints for the individual sonic measurements are not easily computed as flows are more complex. Depending on wind flow patterns (e.g. the vortex direction) and turbulence characteristics, the area or volume contributing to the flux must change. However, due to the strong vertical mixing it is believed that in the vertical, footprints for the individual sonics will be relatively consistent between measurements under the same flow conditions. Even if the along-canyon dimension of the footprint changes, assuming the temperature changes relatively slowly in this direction, the measured flux could show a relation with the different surfaces in and above the canyon. To some

extent this can be tested by comparing the measurements against a simple model to generate fluxes from the various surfaces. Modelled kinematic heat flux density is calculated as:

$$H = \frac{\Delta T}{r} \quad (1)$$

with the resistance to heat transfer assumed to be ten times that for momentum i.e.,

$$r = \frac{10M}{u_*^2} \quad (2)$$

where  $u_*$  and  $M$  represent the measured local friction velocity and total wind speed ( $\sqrt{u^2 + v^2 + w^2}$ ), respectively, and  $\Delta T$  is the difference between the surface and ambient air temperature. The factor of 10 is generally less than that found over bluff bodies at local scales but within the range of observed values (Voogt and Grimmond 2000).

The surface temperatures were spatially averaged to produce single temperatures for the roof, canyon, and east and west walls. A complete surface temperature average was then computed from the roof and canyon components based on their relative surface areas (plan area fraction of roof = 0.6). The wind and turbulence statistics from R4, C4, E4, and W4 were used with Eqs. (1) and (2) to model above, canyon top, east and west fluxes, respectively. For the road exchange, sonic measurements at C2 were used in conjunction with  $T_{\text{road}}$  to compute the modelled flux.

## 2.5 Buoyancy effects on flow

Buoyancy effects on flow may have a significant impact on the transport of air pollution or hazardous materials within and from the canyon, however, these effects are difficult to quantify. The ‘observed’ buoyancy effect will be examined in Sect. 3.3 by comparing flow under ‘heated’ and ‘non-heated’ conditions. Cases will be selected first based on diurnal heating patterns, and secondly, by Froude number.

The Froude number (Fr) can be used to examine the relative importance of buoyancy effects on flow, such that with  $\text{Fr} < 1$ , the buoyancy force exceeds the inertial force. Here Fr is defined, following Kovar-Pankus et al. (2002), as:

$$\text{Fr} = M_{\text{R4}}^2 / (gz_{\text{H}}(T - T_{\text{R4}})/T_{\text{R4}}) \quad (3)$$

where  $M_{\text{R4}}$  and  $T_{\text{R4}}$ , are the ambient wind speed ( $\text{m s}^{-1}$ ) and air temperature (K), respectively at R4,  $T$  is the temperature (K) of the surface in question (i.e. for  $\text{Fr}_{\text{west}}$ ,  $T$  is the west wall temperature),  $g$  is the acceleration due to gravity, and  $z_{\text{H}}$  is the canyon height (m), which is the maximum length scale of the effect.

## 3 Results and discussion

### 3.1 Temperature distribution

Under clear skies, surface temperatures within the canyon follow the pattern expected due to solar radiation loading both diurnally and seasonally. In summer (Fig. 2a), both walls are in direct sunlight over their entire heights for at least a couple of hours. Figure 3 shows the temperature response of the walls based on surface-to-air temperature differences ( $\Delta T$ ). The sheet metal surface of the roof, which also covers the uppermost

2 m of the canyon wall surface (to 13 m), heats quickly to temperatures well above ambient ( $\Delta T > 30^\circ\text{C}$  on occasions). The patterns in Figs. 2 and 3 show few differences between modelled shortwave loading and  $\Delta T$ ; most markedly, the highest  $\Delta T$  is limited to the vertical extent of the metal surface with its high thermal admittance, whereas the  $K \downarrow$  maxima cover a greater vertical extent. Further differences in surface temperatures and  $K \downarrow$  may be due to ignoring reflected shortwave, but this is not immediately obvious. Below 13 m the brick surface heats up for less and otherwise follows the pattern of solar loading. Slightly before midday, the east wall begins to receive direct solar radiation starting at street level, and the heating moves up the east wall. The daytime impact of longwave exchange between the walls is most evident in the afternoon, after the west wall has cooled slightly (Fig. 3a). The west wall temperatures then show a secondary peak (local maximum) due to the emitted longwave radiation from the east wall. The east wall shows a morning local maximum, albeit weaker, again presumably due to the emitted longwave from the opposite wall.

At night the surface temperature variation with height is due to the variation in net longwave radiation ( $L^*$ ) with height, which itself primarily results from differences in view factors. In summer, nighttime  $L^*$  increases with decreasing height down into the canyon, from  $-100 \text{ W m}^{-2}$  above the canyon ( $\psi_s = 1$ ) to  $-54 \text{ W m}^{-2}$  at 6 m ( $\psi_s = 0.37$ ). Measured exchange ( $L^*$ ) from the canyon walls at 6 m was  $-8$  and  $-13 \text{ W m}^{-2}$  for the west and east walls, respectively. Temperatures decrease with height toward the canyon top but are very similar ( $< 2.5^\circ\text{C}$  difference) within the lowest 12 m of the canyon. Lower than ambient temperatures are recorded for the sheet metal roof including the portions in the upper portion of the canyon for most of the night. In the early morning the lower portions of the walls may also be slightly cooler ( $0$ – $2.5^\circ\text{C}$ ) than ambient.

The patterns for the spring and autumn periods are similar to those in summer with the expected differences due to changes in solar forcing. The nighttime period is longer and there is a smaller range of absolute temperature differences despite the internal building heating (Fig. 3b). Also over this period mean surface temperatures in the canyon do not fall below ambient. In winter the west wall receives almost no direct radiation below 14 m. Differences in temperature with height throughout the day and night are consequently small ( $< 2.5^\circ\text{C}$ , Fig. 3c). The walls of the east building are noticeably warmer than those of the west building. This also occurs at night in the other seasons, but not necessarily for the same reason. In the late day and early night such a difference is expected. The east wall's aspect is slightly south-west, and therefore it receives more solar input. By early morning the longwave exchange between the walls and sensible heat losses have brought them to the same temperature. In the winter period the differences persist throughout the diurnal cycle and are therefore more likely due to the poor insulation in the east wall building.

Compared to the surface temperature, the daytime air temperature field seems more complex (Fig. 4). Shortly after sunrise, above-canyon air temperature rises faster than air temperature in the canyon. In summer, this can result in a slightly stable potential temperature profile from the canyon to the air above. In the spring/autumn periods the solar forcing is weaker and the canyon air remains warmer except near the roof. However, by mid morning the canyon air is from 0.5 to  $2^\circ\text{C}$  warmer than ambient and with a peak at slightly above 0.5 H; later in the day the temperature peak moves upward. For all seasons, the peak air temperature difference corresponds to the peak surface-to-air temperature difference for the east wall at a height of 14 m and the location of peak solar radiation loading. Kanda et al. (2005) also found that

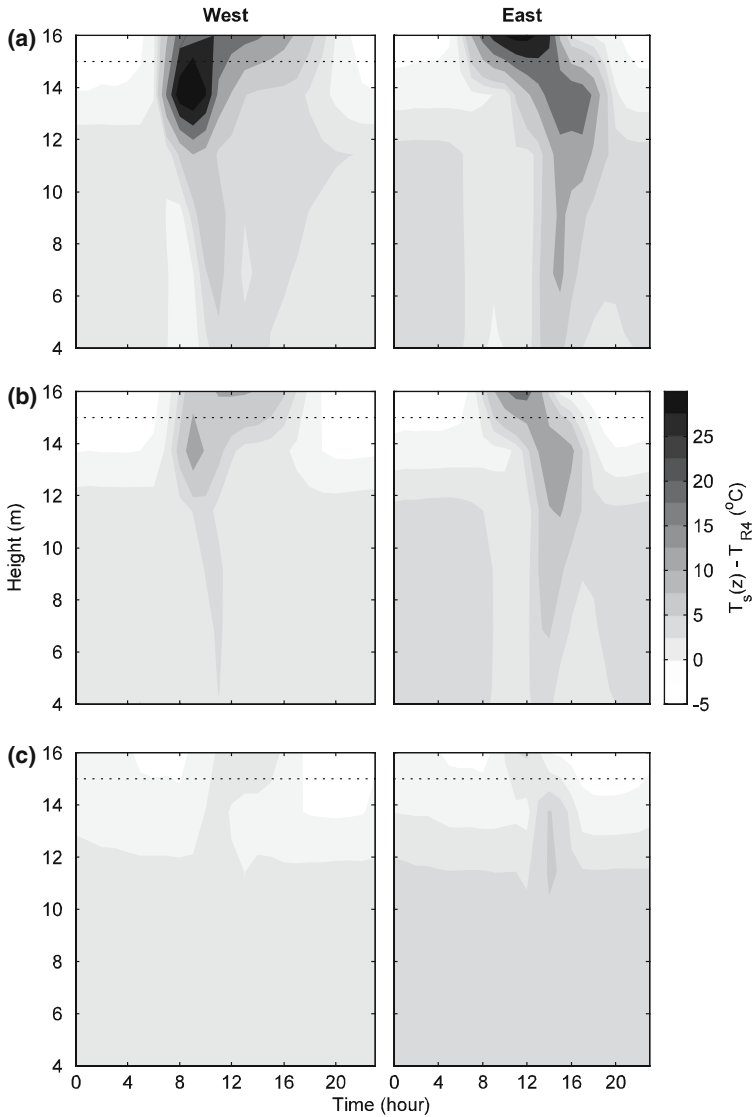
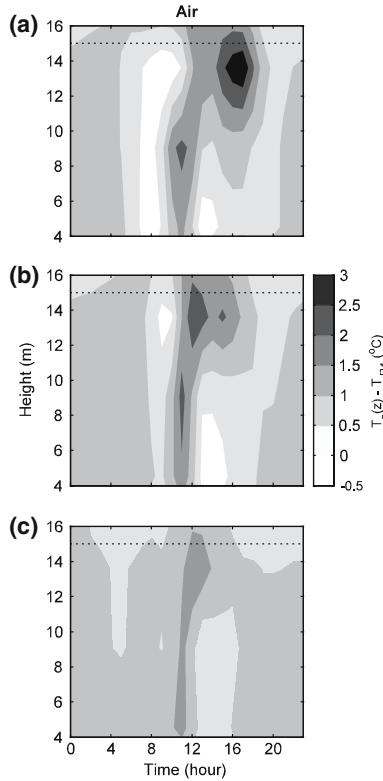


**Fig. 3** Surface temperatures in the canyon as a mean difference from R4 for sunny days in each subset as in Fig. 2: **(a)** summer, **(b)** spring and autumn, **(c)** winter. The line marks the canyon top

peak air temperatures in an urban canopy (mean building height = 7.3 m) correspond to the location of maximum solar radiation absorption. In that case it moved seasonally from roof level (winter) to near ground level (summer). Here the peak loading is relatively constant near roof height (Fig. 2) as is the air temperature peak due to the latitude and canyon depth. At the same time as the afternoon air temperature peak, slightly cooler temperatures develop lower in the canyon. These patterns do not perfectly reflect changes in surface temperature due to the impacts of wind flow and turbulent mixing within the canyon.

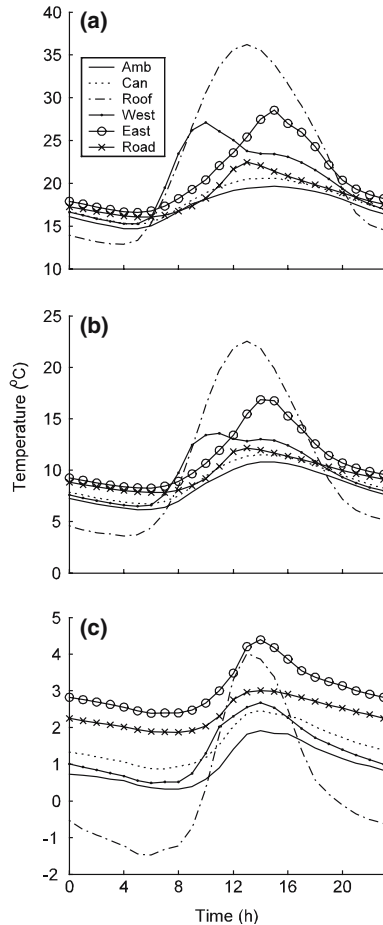
**Fig. 4** Air temperatures in the canyon as a mean difference from R4 for sunny days in each subset as in Fig. 2: (a) summer, (b) spring and autumn, (c) winter. The line marks the canyon top. All air thermocouples were used to calculate the mean vertical temperature profile i.e. horizontal variation within the canyon is ignored



### 3.2 Heat fluxes and surface temperatures

Based on seasonal averages of all-sky conditions, the surface, excluding the roof, and the canyon air are nearly always warmer than ambient both day and night (Fig. 5). This generates positive heat fluxes from the canyon to the overlying atmosphere (Fig. 6). Most notably on summer nights the walls are between 5 and 7°C warmer than the roof, though only slightly warmer than ambient. Thus the canyon walls are a likely source of positive heat fluxes at night. This is true for all seasons although the temperature contrasts are not as great as in summer. Despite the limitation of considering only vertical turbulent transport, the heat fluxes tend to follow the values modelled using the simple resistance formulation. The measurements should not follow one source (e.g. wall) perfectly as the turbulence in the canyon is mixing heat upward, or outward, from all exchanging surfaces as well as advected heat from outside the canyon. For example, the flux measured at E4 rises before the east wall has been heated and is therefore incorporating heat from some other surface. The fluxes measured at C4 and C2 show relatively good agreement with the patterns from the modelled Eq. (1) release from the total canyon surface and the lower canyon surface, respectively. Even the above-canyon measurements tend to follow the flux from the average surface. However, fluxes measured on the west side (e.g. W4 in Fig. 6) depart considerably from the modelled values, showing a much higher value with less diurnal variation. In part this can be attributed to the three dimensionality of the heat transport, which

**Fig. 5** Mean diurnal ambient (Amb, measured at R4) and canyon air temperature (Can) and spatially averaged surface temperatures for roof, walls (west, east) and road for all sky conditions by season **(a)** summer ( $N = 3648$ ), **(b)** spring and autumn ( $N = 4392$ ), **(c)** winter ( $N = 2184$ ).  $N$  is the number of observations for each subset



is here considered in only one dimension, and the complexity of advective transport within the canyon. To give one example, the turbulent flux component directed perpendicularly away from the walls can be greater than the vertical component. Multiple linear regression analysis was used to quantitatively examine the relation between the modelled and measured fluxes with the results for westerly flow shown in Table 1. As with Fig. 6, there is much better agreement for the east and centre measurement locations than for the west. The relative importance of  $H_{\text{east}}$  and  $H_{\text{road}}$  increases, as expected, from west to east and from top to bottom, respectively. Under this situation, vertical mixing is relatively strong in the east and centre and along-canyon and across-canyon components are less a factor. The roof flux component does not decrease monotonically with height as it is influenced by the collinearity of  $H_{\text{road}}$ . Under westerly flow, and in general, heat fluxes from the west side are smaller and show a weaker relation with the model (Table 1). With easterly flow the situation somewhat reverses itself with better agreement from east to west, although not to the same degree as westerly flow (not shown). The west wall contributes only 14% of the flux at W4 under an easterly flow versus 70% for the east wall at E4 under a westerly flow.

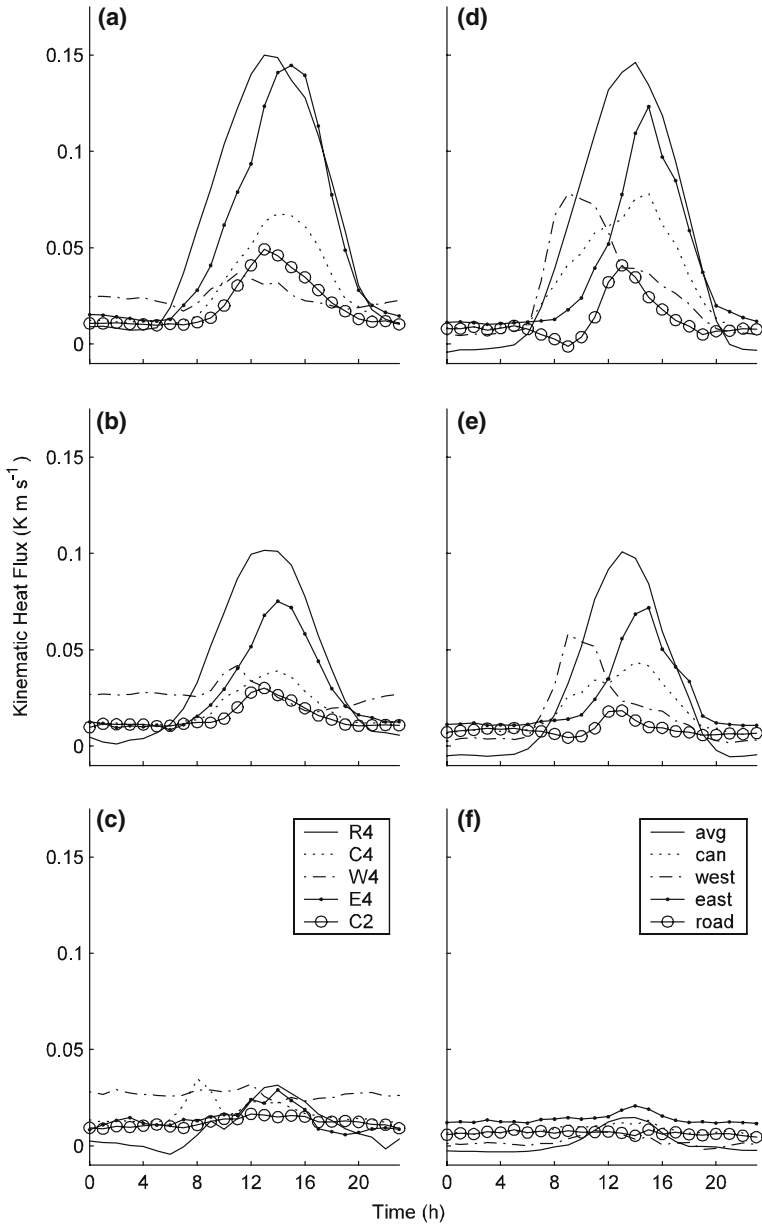


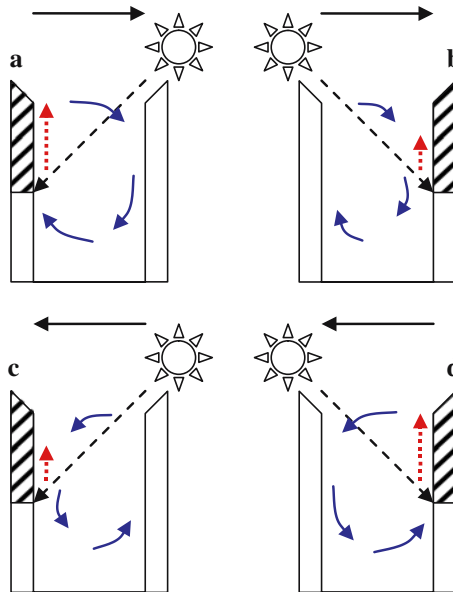
**Fig. 6** Measured vertical (a–c) and modelled (d–f) kinematic heat flux for all sky conditions by season as in Fig. 5: (a&d) summer, (b&e) spring and autumn, (c&f) winter. Measured flux labels refer to sonic locations and modelled flux labels represent the spatially averaged surface temperature used to calculate the flux as in Fig. 5 except ‘avg’, which represents the spatial mean (area weighted) of roof and canyon temperatures

**Table 1** Linear regression coefficients ( $H_z = b_0 + b_{\text{roof}}H_{\text{roof}} + b_{\text{west}}H_{\text{west}} + b_{\text{east}}H_{\text{east}} + b_{\text{road}}H_{\text{road}} + \varepsilon$ ) for the relation between observed kinematic heat flux ( $H_z = w'T'_v$ ) for individual sonics with modelled fluxes (Eq. 1 for each facet)

Sonic	N	$b_0$	$b_{\text{roof}}$	$b_{\text{west}}$	$b_{\text{east}}$	$b_{\text{road}}$	$R^2$	RMSE ( $\text{K m s}^{-1}$ )
W4	2062	1.38	-0.18	-0.81	0.34	0.27	0.36	0.01
W3	2066	0.89	0.09	0.19	-0.52	0.35	0.21	0.01
W2	1486	0.93	0.26	0.12	-0.86	0.50	0.13	0.02
C4	2066	0.18	0.18	-0.01*	0.60	0.04	0.74	0.02
C3	2063	0.28	0.21	0.04	0.31	0.16	0.77	0.01
C2	2065	0.35	0.21	-0.02*	0.20	0.25	0.81	0.01
E4	2066	0.05	0.17	0.12	0.66	-0.01*	0.85	0.03
E3	2024	0.17	0.14	0.08	0.49	0.12	0.87	0.02
E2	2066	0.30	0.14	0.01	0.36	0.18	0.68	0.02

Results given for westerly flow, non-winter days, and wind speed  $> 2 \text{ m s}^{-1}$ .  $N$  is the number of hourly observations. Coefficients are normalized to mean observed  $H_z$  for comparison. \*Not significantly different from 0 (95% confidence interval). Fit statistics of  $R^2$  (coefficient of determination) and RMSE (root mean square error) are given

**Fig. 7** Schematic of flow and canyon heating classification. (a) westerly, AM; (b) westerly, PM; (c) easterly, AM; (d) easterly, PM. The solid vectors show the typical vortex circulation modified by the buoyancy flow (dotted). The hatched portion highlights the sunlit portion of the surface



### 3.3 Influence of wind on temperature distribution within the canyon and vice-versa

The effects of buoyancy on flow patterns may not be immediately obvious and changes with ambient wind direction. One possible interpretation of the influence of wall heating on flow within the canyon is shown in Fig. 7. The portion of the wall that is sunlit warms rapidly in comparison to the canyon air and can generate upward motion near the wall. This motion may persist from some distance away from the wall, particularly if the leeward wall is heated (Kovar-Pankus et al. 2002). If the windward wall is heated this may give rise to a secondary vortex (not drawn) as the buoyant flow counteracts the usual vortex pattern, as was demonstrated by Louka et al. (2002).

Since the measurements occur relatively distant from the walls of the canyon, it was not possible to measure the complete extent to which surface heating influences the motion of air within the canyon. Instead we compare cases in Fig. 7 such that the differences should be associated with the different heating patterns. Figure 8 shows the mean wind vectors ( $x$ - $z$  plane) and temperature distribution for sunny non-winter days grouped by the situations given in Fig. 7. The flow patterns for the comparable cases are very similar (Figs. 8a–d), however there are discernable differences in the mean flow field when individual measurements were normalized to ambient wind speed for comparison (Figs. 8e, f). In Fig. 8e an enhanced circulation pattern is accompanied by above-canyon flow around the same magnitude, hence it cannot be inferred that the differences are due solely to buoyancy effects. In Fig. 8f, where the vortex should be weakened or shifted, the differences cannot be attributed to above-canyon flow, but the differences are very small ( $< 0.1 \text{ m s}^{-1}$ ). There is no evidence for a secondary vortex near the windward heated wall that extends out to the measurement locations, as has been shown in numerical experiments.

The differences in flow due to buoyancy effects should be enhanced if the data are restricted to low Froude numbers and thus more readily seen. Fig. 9 shows similar cases to Figure 8 except that the time of day comparison is replaced with the comparison between low and high Froude numbers for the west wall surface. These low  $Fr_{\text{west}}$  cases occur primarily when wind speeds are low, and not when temperature gradients are largest. Thus under these situations, the wall-to-air temperature gradient is weaker than in Fig. 8. With westerly flow and west wall heating, the enhancement of the upward flow near the west wall is stronger than in Fig. 8e ( $> 0.1 \text{ m s}^{-1}$ ). However, there seems to be no overall vortex enhancement. Figure 9e suggests the downdraft on the east side of Fig. 9a is weaker than that in Fig. 9b when it is expected to be slightly enhanced. In Fig. 9c, where the buoyancy effect opposes the vortex, there is a slightly enhanced vortex from the more typical easterly flow situation (Fig. 9f). This is apparently different from what was expected based on low Froude number experiments (Kovar-Panskus et al. 2002; Louka et al. 2002). The relative upward motion, if it exists, must be confined to a layer much nearer the wall than was measured. The apparent enhancement could be due to a relatively stronger vortex at the lower wind speeds in low Froude number cases. Although this is a very limited part of the overall data, it is somewhat surprising that there is no obvious effect of the heated downstream wall on air flow but this is actually in agreement with the observed behaviour of released balloons (Kovar-Panskus et al. 2002) and wind observations (Louka et al. 2002). Louka et al. (2002) noted that their numerical experiment overestimated the thermal effects of wall heating leading to a secondary vortex covering much more of the canyon than was possible given observations.

In contrast, the temperature distribution is affected by the flow in more obvious ways. With ambient flow toward the heated wall (Figs. 8b, c), the gradient within the canyon is not as great. This is to be expected as turbulent mixing is enhanced near the windward wall relative to the leeward wall (Eliasson et al. 2005) and some cooler air from above the roof is mixed downward. Thus, in the cases of flow against the non-heated wall (Figs. 8a, d), stronger gradients in air temperature are possible and some penetration of cooler air from aloft seems likely. On the leeward side any inflow from aloft is also heated owing to the aspect of the roof. These differences are readily seen in the changes in direction and magnitude of the turbulent fluxes (Fig. 8). Near the leeward wall  $H$  is weak and directed away from the wall in the direction of the temperature gradient. Near the windward wall,  $H$  is directed upward and is of a larger

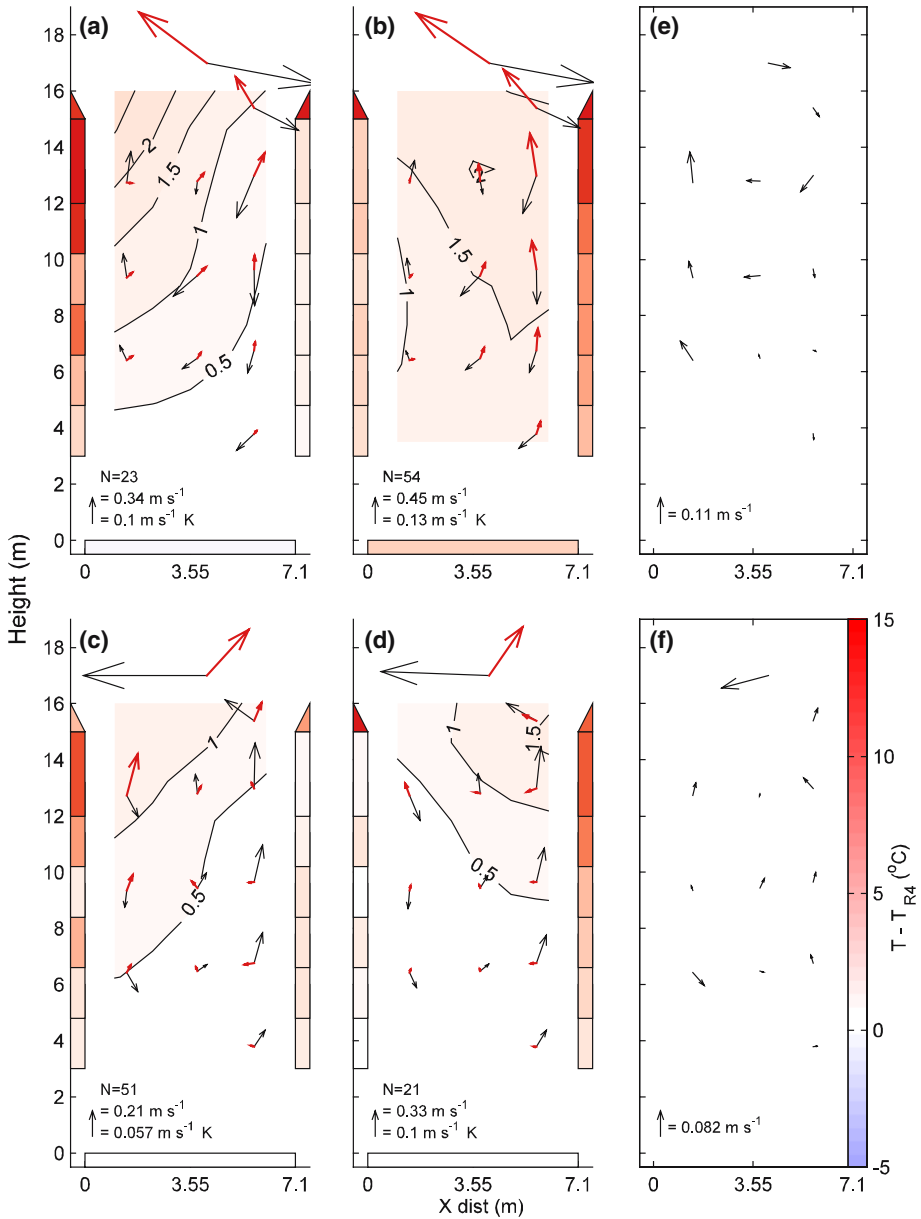


**Fig. 8** Mean temperature difference from R4 (filled contours for air temperature and patches for wall surface temperature), wind vectors ( $u_i$  where  $i = x$  or  $z$ , black/light arrows) and turbulent flux vectors ( $H_i = \overline{u_i T'_v}$ , red/bold arrows) for cases (a–d) shown in Fig. 7. The right hand column (e & f) shows the mean vector difference between normalized mean wind fields. Vector lengths are normalized to mean wind speed or  $w'T'_v$  at R4. Temperature scale applies to (a–d); no temperatures are shown in (e & f).  $N$  is the maximum number of observations as some instruments (e.g. C6) were not available for the entire period

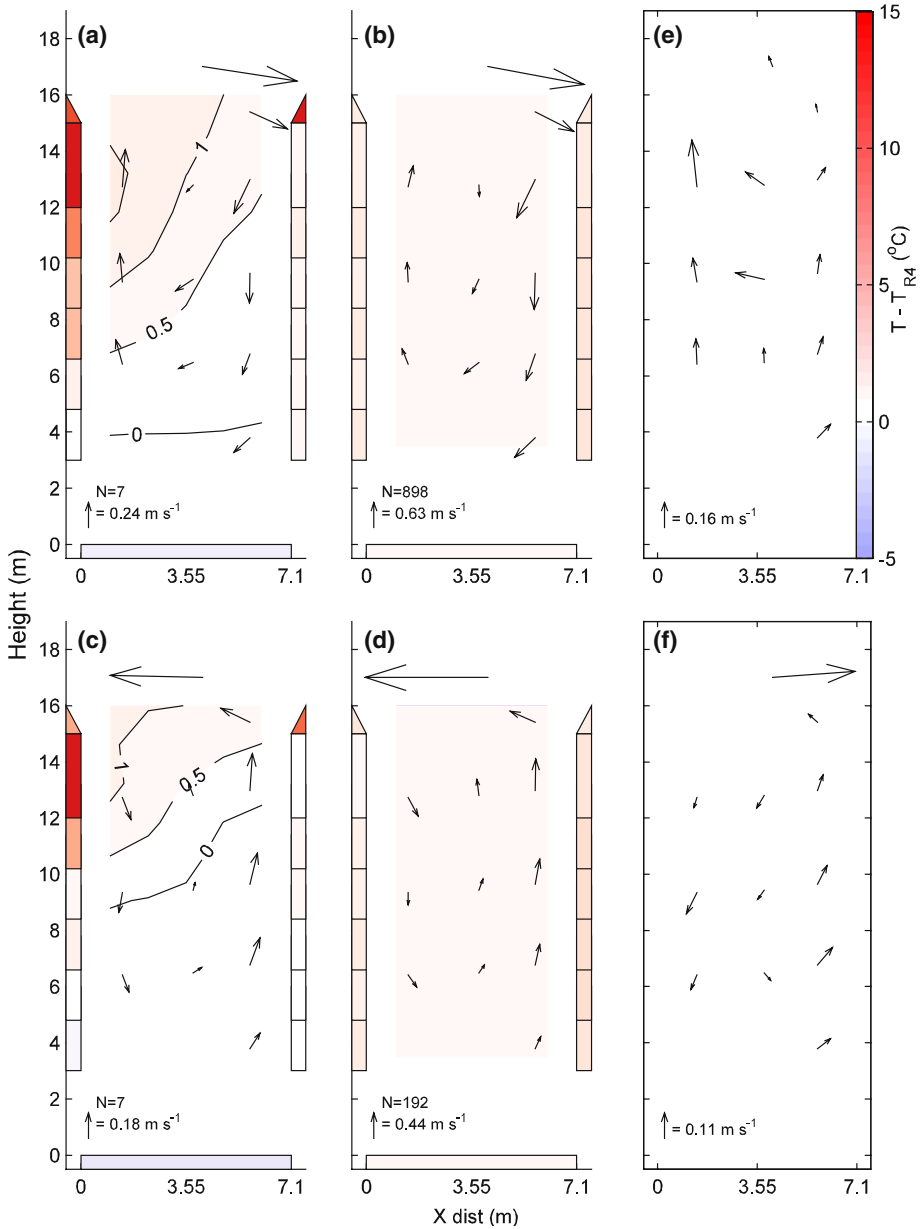


**Fig. 9** Mean temperature difference from R4 (filled contours for air temperature and patches for wall surface temperature) and wind vectors ( $u_i$  where  $i = x$  or  $z$ , black/light arrows) for cases stratified by Froude number: **(a)**  $Fr_{west} < 1$ , westerly flow; **(b)**  $Fr_{west} > 10$ , westerly flow; **(c)**  $Fr_{west} < 1$ , easterly flow; **(d)**  $Fr_{west} > 10$ , easterly flow. For all cases,  $Fr_{east} > 10$ . **(e & f)** show the mean vector difference between normalized mean wind fields. Vector lengths are normalized to mean wind speed at R4

magnitude than near the upstream wall, even when the windward wall is not heated (Figs. 8a, d). The differences in the turbulent heat fluxes between the windward and leeward walls are greater than the factor of 2 suggested by Harman et al. (2004b). When the leeward wall is heated, presumably a large quantity of heat is advected out of the canyon in a thin layer near the walls. However, this seems to have less impact on the overall turbulent flux out of the canyon. The direction and relative magnitude of the turbulent flux at C6 changes little with respect to which wall is heated. The strong shear layer at the top of the canyon effectively averages the advective and turbulent components from within the canyon. The patterns in  $H$  also show the expected dependence on vertical position within the canyon, with flux densities increasing toward the top of the canyon.

#### 4 Concluding comments

Geometry is a crucial factor in determining not only flow but also temperature distributions in urban canyons. The daytime pattern of surface temperature follows both diurnal and seasonal patterns of incoming solar radiation determined solely by geometry. The most general daytime clear sky heating patterns can be reproduced without resorting to considering reflections or within-canyon exchange. However, this notably ignores the longwave exchange that heats the west wall in the afternoon. Eddy covariance turbulent heat flux measurements within a street canyon are limited in their interpretability due to the changing footprints and three-dimensional nature of the flux. Here it was shown that fluxes could be consistent between measurements with respect to a model that was a linear combination of fluxes from the roof, walls, and street determined by a simple resistance formulation. There are large spatial differences for measured fluxes within the canyon dependent on whether the windward or leeward wall is heated, although the strong shear layer at the canyon top effectively mixes the heat so there is no apparent difference in the fluxes from the entire canyon.

Within the canyon when the windward wall is heated, mixing and turbulent heat fluxes are enhanced possibly due to the interaction of buoyancy with the normal vortex circulation, and the entrainment of cooler air. When the leeward wall is heated, it appears that the heat transfer is much more concentrated near the wall. Thus heat can be transported primarily vertically without being mixed outward into the canyon. When this buoyant flow encounters the cross-canyon flow and the shear layer at the canyon top it becomes well mixed, so that some of this buoyant flow will be recirculated. These results support general resistance network formulations commonly found in urban surface parameterizations. If canopy layer exchanges are not of interest the direction of flow with respect to heating is of less consequence. Thus modelling canyon heat fluxes from a single averaged wall temperature may be sufficient. Although the road surface was not an important source of non-winter heat fluxes here, this result is conditioned on the street orientation, the high canyon aspect ratio, and high latitude.

The difference in canyon air heating in the cases of perpendicular flow may have more practical consequences for modelling pollution dispersion and identifying potential hot spots. In a review of air quality modelling in street canyons, Vardoulakis et al. (2003) note that the problem of thermal effects due to solar radiation is one area that requires future research attention. Flow patterns were examined under differential heating to assess whether buoyancy effects on flow were observable. In general these were either unobservable in the data examined or much weaker than expected given

the results of published numerical experiments. However, even though no secondary circulation was seen to form, there was some evidence that the measurements demonstrate buoyancy effects from the heated walls. There is clearly a need for further investigations of flow near heated walls.

**Acknowledgements** The project was financially supported by the Knut and Alice Wallenberg Foundation and FORMAS – the Swedish Research Council for Environment, Agricultural Sciences and Spatial Planning.

## References

- Aida M (1982) Urban albedo as a function of the urban structure – a model experiment (Part I). *Boundary-Layer Meteorol* 23:405–413
- Aida M, Gotoh K (1982) Urban albedo as a function of the urban structure – a two-dimensional numerical simulation (Part II). *Boundary-Layer Meteorol* 23:415–424
- Arnfield AJ (1982) An approach to the estimation of the surface radiative properties and radiation budgets of cities. *Phys Geogr* 3:97–122
- Arnfield AJ (2003) Two decades of urban climate research: a review of turbulence, exchanges of energy and water, and the urban heat island. *Int J Climatol* 23:1–26
- Baik J-J, Kim J-J (1999) A numerical study of flow and pollutant dispersion characteristics in urban street canyons. *J Appl Meteorol* 38:1576–1589
- Best MJ (2005) Representing urban areas within operational numerical weather prediction models. *Boundary-Layer Meteorol* 114:91–109
- Christen A, Vogt R (2004) Energy and radiation balance of a central European city. *Int J Climatol* 24:1394–1421
- Dabbert WF, Ludwig FL, Johnson WB Jr (1973) Validation and applications of an urban diffusion model for vehicular pollutants. *Atmos Environ* 7:603–618
- Eliasson I, Offerle B, Grimmond CSB, Lindqvist S (2005) Wind fields and turbulence statistics in an urban street canyon. *Atmos Environ* 40:1–16. DOI: 10.1016/j.atmosenv.2005.03.031
- Grimmond CSB, Salmund JA, Oke TR, Offerle B, Lemonsu A (2004) Flux and turbulence measurements at a dense urban site in Marseille: heat, mass (water, carbon dioxide) and momentum. *J Geophys Res Atmos* 109 (D24101):1–19. DOI: 10.1029/2004JD004936
- Harman IN, Best MJ, Belcher SE (2004a) Radiative exchange in an urban street canyon. *Boundary-Layer Meteorol* 110:301–316
- Harman IN, Barlow JF, Belcher SE (2004b) Scalar fluxes from urban street canyons. Part II: model. *Boundary-Layer Meteorol* 113:387–409
- Kanda M, Moriawaki R, Kimoto Y (2005) Temperature profiles within and above an urban canopy. *Boundary-Layer Meteorol* 115:499–506. DOI: 10.1007/s10546-004-5644-5
- Kim J-J, Baik J-J (2001) Urban street-canyon flows with bottom heating. *Atmos Environ* 35:3395–3404
- Kondo A, Ueno M, Kaga A, Yamaguchi K (2001) The influence of urban canopy configuration on urban albedo. *Boundary-Layer Meteorol* 100:225–242
- Kovar-Panskus A, Moulinneuf L, Savory E, Abdelqari A, Sini J-F, Rosant J-M, Robins A, Toy N (2002) A wind tunnel investigation of the influence of solar-induced wall-heating on the flow regime within a simulated urban street canyon. *Water, Air, Soil Poll: Focus* 2:555–571
- Kusaka H, Kondo H, Kikegawa Y, Kimura F (2001) A simple single-layer urban canopy model for atmospheric models: comparison with multi-layer and slab models. *Boundary-Layer Meteorol* 101:329–358
- Louka P, Vachon G, Sini J-F, Mestayer PG, Rosant J-M (2002) Thermal effects on the airflow in a street canyon – Nantes’99 experimental results and model simulations. *Water, Air, Soil Poll: Focus* 2:351–364
- Martilli A, Clappier A, Rotach MW (2002) An urban surface exchange parameterisation for mesoscale models. *Boundary-Layer Meteorol* 104:261–304
- Masson V (2000) A physically-based scheme for the urban energy balance in atmospheric models. *Boundary-Layer Meteorol* 94:357–397
- Masson V, Grimmond CSB, Oke TR (2002) Evaluation of the town energy balance (TEB) scheme with direct measurements from dry districts in two cities. *J Appl Meteorol* 41:1011–1026
- Nakamura Y, Oke TR (1988) Wind, temperature and stability conditions in an east-west oriented urban canyon. *Atmos Environ* 22:2691–2700

- Nunez M, Oke TR (1977) The energy balance of an urban canyon. *J Appl Meteorol* 16:11–19
- Offerle B, Grimmond CSB, Fortuniak K, Klyzik K, Oke TR (2006) Temporal variations in heat fluxes over a central European city centre. *Theor Appl Climatol* 84: 103–116
- Oke TR (1987) *Boundary layer climates*. Routledge, 435 pp
- Sailor DJ, Fan H (2002) Modeling the diurnal variability of effective albedo for cities. *Atmos Environ* 36:713–725
- Salmund JA, Oke TR, Grimmond CSB, Roberts S, Offerle B (2005) Venting of heat and carbon dioxide from urban canyons at night. *J Appl Meteorol* 44:1180–1194
- Schmid HP (2002) Footprint modeling for vegetation atmosphere exchange studies: a review and perspective. *Agric For Meteorol* 113:159–184
- Schotanus P, Nieuwstadt FTM, DeBruin HAR (1983) Temperature measurement with a sonic anemometer and its application to heat and moisture fluctuations. *Boundary-Layer Meteorol* 26:81–93
- Sini J, Anquetin S, Mestayer P (1996) Pollutant dispersion and thermal effects in urban street canyons. *Atmos Environ* 30:2659–2677
- Vachon G, Rosant J-M, Mestayer P, Sini J-F (1999) Measurements of dynamic and thermal field in a street canyon, URBCAP Nantes 99. In: *Proceedings of the 6th international conference on harmonisation within atmospheric dispersion modelling*, Rouen, France, October 11–14, 12 pp
- Vardoulakis S, Fisher BEA, Pericleous K, Gonzalez-Flesca N (2003) Modelling air quality in street canyons: a review. *Atmos Environ* 37:155–182
- Voogt JA, Grimmond CSB (2000) Modeling surface sensible heat flux using surface radiative temperatures in a simple urban area. *J Appl Meteorol* 39:1679–1699
- Voogt JA, Oke TR (1998) Effects of urban surface geometry on remotely-sensed surface temperature. *Int J Remote Sens* 19:895–920